Korean J. Chem. Eng., 37(12), 2340-2350 (2020)
DOI: 10.1007/s11814-020-0644-9

pISSN: 0256-1115
eISSN: 1975-7220

Preparation of epoxypropyl functionalized graphene oxide and its anticorrosion properties complexed with epoxy resin

Xiaofeng Yang*,†, Yuepeng Zhang*, Zhiping Chen*, Yinshuai Yang, Hongxia Jing*, Zhenhao Sun*, and Huijie Wang***

*School of Science, North University of China, Taiyuan 030051, China
**School of chemical Engineering, Dalian Univesity of Technoloy, Dalian 116024, China
(*Received 17 April 2020 • Revised 2 July 2020 • Accepted 19 July 2020*)

Abstract−Functionalized graphene oxide (GO)/epoxy resin (EP) composite coating has attracted attention due to its advantages of epoxy resin in acid resistance, anticorrosion and having the characteristics of GO such as good chemical stability and strong electrolyte barrier properties. In this study, epoxypropyl functionalized graphene oxide (EFGO) was synthesized with a new strategy by grafting epichlorohydrin (ECH) onto the surface of GO. EFGO was then cross-linked with EP by diethylenetriamine (DETA) to fabricate EFGO/EP anticorrosive coating. The structure and property of EFGO and EFGO/EP were characterized and evaluated by various methods such as FTIR, Raman, XPS, SEM, and EIS. The results showed that the graft amount of epoxypropyl on GO surface could be effectively increased by using KI-KF catalysis system. The increase of the graft amount further improved the compatibility between EFGO and EP. EFGO/EP had a network structure with EFGO as the "central node". The "central node" locked the movement of EP chain segment, as improving the thermal stability of EFGO/EP. The EFGO/EP coating fabricated by the EFGO, which grafted larger epoxypropyl, had good anticorrosion performance and adhesion with steel plates, showing a good barrier effect on electrolyte migration. The coating resistance reached up $4.88\times10^8\ \Omega\ cm^2$.

Keywords: Epoxypropyl, Functionalized Graphene Oxide, Epoxy Resin, Anticorrosion

INTRODUCTION

Organic coatings including epoxy resin (EP) are widely used in heavy-duty anticorrosive coatings with good resistance to acids, alkalis, oil, and corrosion [1-3]. However, pure EP materials intrinsically have the disadvantages of poor heat resistance, poor impact resistance and electrolyte permeability [4]. Graphene (Gr) and its derivatives have attracted much attention due to high thermal and chemical stability, large specific surface area, and barrier properties [5,6]. And the above characteristics of Gr and its derivatives could complement the intrinsic disadvantages of EP. Therefore, development of anticorrosion coating based on graphene-epoxy composite has become a new direction in the field of anticorrosion [7]. For example, Gr/EP composite antiseptic coating [8] could be obtained by mixing water-based epoxy resin with Gr water dispersion, which was acquired by ultrasonic method. The results showed that the coating resistance reached 293 $k\Omega\ cm^2$. When the loading of Gr was 0.5%, the anticorrosion property of composite was increased by 99.7% compared with pure EP coating.

However, there was poor compatibility between Gr and EP. Problems such as migration and exposure of Gr particles are inevitable in the Gr/EP composite coatings fabricated by mechanical mixing. This decreased the long-lasting corrosion resistance property of coating. To solve the above problems, the most common method was to first introduce functional active group onto the surface of graphene to prepare functional graphene (FGO), and then combined with EP to obtain FGO/EP composites with good compatibility.

There are two main strategies for fabrication of FGO at present. The first is by covalently grafting active groups such as NH_2, phosphoric acid and imidazole ionic liquid on the surface of GO [9,10]. For example, P-phenylenediamine was covalently grafted on the surface of GO by Ramezanzadeh et al. [11], and then combined with EP using solvent evaporation method to prepare FGO/EP coatings. The resistance of the coating reached 7,300 $M\Omega cm^2$. After soaking the coating in 3.5 wt% NaCl solution for 20 days, the impedance values maintained about 61% of the original impedance values. For another example, N-(3-aminopropyl)-imidazole ionic liquid (IL) was used to modify GO by Liu et al. [12] to obtain IL-GO. And then IL-GO was combined with EP to fabricate IL-GO/EP composite coating. Both compatibility of GO with EP and corrosion durability of IL-GO/EP composite coatings were improved effectively. However, the modifiers of organic amine were highly toxic, and the reaction needed to take place in an inert atmosphere. In particular, the amine groups on FGO partly played a curing agent role during curing process, the effect of curing limited the controllability of coating preparation.

The second strategy was grafting function groups, which were not reacting with EP (such as epoxy groups), on the surface of GO to obtain FGO. For example, 3-glycidoxypropyltrimethoxysilane (GPTMS) containing epoxy group was used by Pourhashem et al. [13] to modify GO to synthesize GPTMS-f-GO. Then, GPTMS-f-GO/EP composites were fabricated by combining GPTMS with EP.

†To whom correspondence should be addressed.
E-mail: yangxiaofeng123@nuc.edu.cn

GPTMS-f-GO/EP coating, exhibiting high adhesion to the substrate and showing long-lasting anticorrosion. The biggest disadvantage of this method was the high cost of GPTMS.

In addition, supramolecular assembly strategies were used to modify GO for few researchers. GO was assembled first with organic molecules in non-covalent bond to form supramolecules. And then the supramolecules were further assembled with each other to form intermediates through in-situ polymerization or π-π stacking. The intermediates had core-shell structure with organic molecules as shell and GO as core. Finally, the intermediates combined with EP to obtain FGO/EP composites. For example, PVP-g-rGO were prepared by Zhang et al. [14] through non-covalent grafting of polyvinylpyrrolidone (PVP) on the surface of reduced graphene oxide (rGO). Then PVP-g-rGO was combined with EP to obtain composite coating, which exhibited good physical shielding properties. However, the coating prepared by this method was prone to produce phase separation due to weak binding force at the supramolecular-EP interface.

In this study, a new strategy was designed and implemented for the preparation of modified functionalized graphene oxide (FGO). Epichlorohydrin (ECH), which is nontoxic, readily available, rich in epoxy groups, was used as raw material and was covalently grafted onto the surface of GO with different catalytic systems to obtain epoxypropyl functionalized graphene oxide (EFGO). On this basis, EFGO and EP were crosslinked by diethylenetriamine (DETA) to obtain an EFGO/EP composite coating. The influences of the content of epoxy group of EFGO on compatibility of EFGO with EP and on the anticorrosion property of EFGO/EP composite coating were studied systematically. The results of this study built up a foundation for the fabrication and development of new FGO/EP composites coatings with good compatibility.

EXPERIMENT

1. Materials

Natural flake graphite (500 mesh) was purchased from Nanjing Quanxi Chemical Co., Ltd. Epoxy resin (E44 type Diglycidyl ether of bisphenol A) was purchased from SINOPEC. DETA, n-butanol and xylene were purchased from Tianjin Kaitong chemical reagent Co., Ltd. N,N-dimethylformamide (DMF), ECH and dodecylbenzene sulfonate were obtained from Tianjin Shentai Chemical Reagent Co., Ltd. Other reagents were purchased from Sinopharm group Co., Ltd. All reagents except for graphite flakes and epoxy resin were analytical grade and used without other treatment.

2. Synthesis of GO

GO was synthesized according to modified Hummers method [15]. 1 g flake graphite was added into mixture of 180 mL H_2SO_4 and 20 mL H_3PO_4, mechanically stirred for 30 min. Then 6 g $KMnO_4$ was added slowly into suspension. The mixture was stirred at 35 °C for 72 h until brownish product was obtained, then poured onto ice. 30% H_2O_2 was added dropwise until the solution was bright yellow. The mixture was centrifuged at 1,000 rpm for 15 min to obtain the solution, then the solution was centrifuged at 4,500 rpm for 4 h to obtain precipitate. Precipitate was washed with 10% HCl and deionized water to get graphite oxide. Graphite oxide was ultrasonicated for 6 h, dialyzed at 30 °C for 3 days in deionized water, freeze-dried for 72 h in turn to obtain GO.

3. Synthesis of EFGO

Two kinds of EFGO were synthesized by nuclephilic substitution reaction between GO and ECH catalyzed with diffrent catalyst. The synthesis of EFGO-1 was catalyzed by KI, and typical process was as follows. 0.2 g GO was disperated for 1 h in 200 mL DMF by means of ultrasonic dispersion to obtain GO dispersion. Then 6 g KI was first added into GO dispersion under stirring, and 40 mL ECH dropwise added in it. The mixture was refluxed at 100 °C for 15 h and then distilled to remove the excess solvent. The residue was washed with water, ethanol and water in turn, then freeze-dried to obtain EFGO-1. The synthesis of EFGO-2 was catalyzed by replacing KI with KI-KF (6 g KI+0.2 g KF), the other synthesis condition and process being equal.

4. Preparation of EFGO/EP Composite

The EFGO/EP composite was fabricated with solvent method [16]. Taking the fabrication of EFGO-1/EP composite as an example, the process was as follows: 0.06 g EFGO-1 was dispersed in 5 mL mixed solvent n-butanol and xylene at a mass ratio of 1 : 3 for 1 h by means of ultrasonic dispersion to obtain EFGO-1 dispersion. 60 g EP was added to 20 mL mixed solvent to obtain epoxy solution. 12 mL DETA was added to 5 mL mixed solvent to obtain curing agent solution. Then EFGO-1 dispersion was further dispersed in epoxy solution first 1 h at a mass ratio 1 : 1,000 to obtain a homogeneous mixture. The homogeneous mixture and curing agent solution were further mixed and stirred for 30 min to obtain EFGO-1/EP composite precursor. Finally, the precursor was poured into a petri dish and cured at room temperature for 24 h and at 100 °C for 2 h to obtained EFGO-1/EP composite. EFGO-2/EP composite was fabricated by substituting EFGO-1 with EFGO-2, the other synthesis condition and process being equal.

To study the thermal stability of EFGO/EP composite, mixtures of EFGO and EP were prepared as comparison samples by mechanical mixing method. The preparation process was shown as follows. The surface of the pure EP was scraped to obtain EP power. The power was ground in a mortar and sifted through a 400 mesh sieve. Subsequently, the EP power was mixed with EFGO at a mass ratio 1 : 1,000, and the mixture was ball milled for 24 h to obtain EFGO-x-m-EP mixtures. When EFGO-1 was used as raw material, the product was named as EFGO-1-m-EP. Analogously, if EFGO-2 was used as raw material, the product was named as EFGO-2-m-EP.

5. Preparation of EFGO/EP Coating

To study the anticorrosive property of EFGO/EP composites, the EFGO/EP coating was prepared on the mild steel by dipping method. The mild steel plate was pretreated by polishing with smooth file and sandpaper, washed with 0.01 g mL^{-1} sodium dodecylbenzene sulfonate solution, deionized water, 20% HCl solution and deionized water, respectively, for 30 min, and dried at 50 °C for 5 min. Subsequently, the mild steel was immersed in precursor prepared as 2.4 for 10 s and removed from precursor for 1 min. The process of immersing for 10 s and removing for 1 min was repeated three times. Finally, the mild steel was clamped on clips, kept at room temperature for 24 h and heated at 100 °C for 2 hours to obtain the coating. The coating was named as EFGO-x/EP coating, x denotes the type of EFGO used to prepare precursor. When the amount of EFGO was zero, the coating was named as EP coating.

6. Characterization

6-1. Structure and Morphology

Functional groups of GO, EFGO and EFGO/EP composites were studied by Fourier transform infrared (FTIR) spectroscopy method in Shimadzu FTIR-8400S infrared spectrometer with a wavenumber range from 500 to 4,000 cm^{-1}. The hybridization state and content of surface elements of GO and EFGO were characterized by Thermo ESCALAB 250XI X ray photoelectron spectroscopy (XPS) analyzer and LabRam HR Evolution Raman spectrometer with λ_{exc}=532 nm respectively.

Crystallinity was tested on Haoyuan DX-2700B X-ray diffractometer using Cu Kα radiation (wavelength=0.154178 nm). Surface morphology was captured by JEOL F7001 scanning electron microscope (SEM). Thermogravimetric (TG) and derivative thermogravimetry (DTG) were conducted by Mettler Toledo TGA1 STAR^e System with a heating rate of 5 °C min^{-1} in N_2. Differential scanning calorimetry (DSC) was studied by Setaram DSC131 calorimeter with a heating rate of 15 °C min^{-1} in N_2.

6-2. Anticorrosion Property

The apparent anticorrosion properties of EFGO/EP coatings were evaluated by electrochemical impedance spectroscopy (EIS) and linear sweep voltammetry (LSV) measure. The measurements were conducted by VSP-300 electrochemical workstation (Bio-logic, France) with three-electrode system including a saturated calomel electrode (reference electrode), platinum electrode (counter electrode) and mild steel with EFGO/EP coating or EP coating (working electrode). The working electrode had a geometrical area of 1 cm^2 opening to the electrolytic solution. 3.5 wt% NaCl was used as electrolyte. The EIS measurements were done at open circuit potential (OCP) in the frequency range of 10^{-2} to 10^5 Hz and at amplitude sinusoidal voltage of ±10 mV at different immersion times. The scan rate of LSV was 5 mV s^{-1}, and the potential range

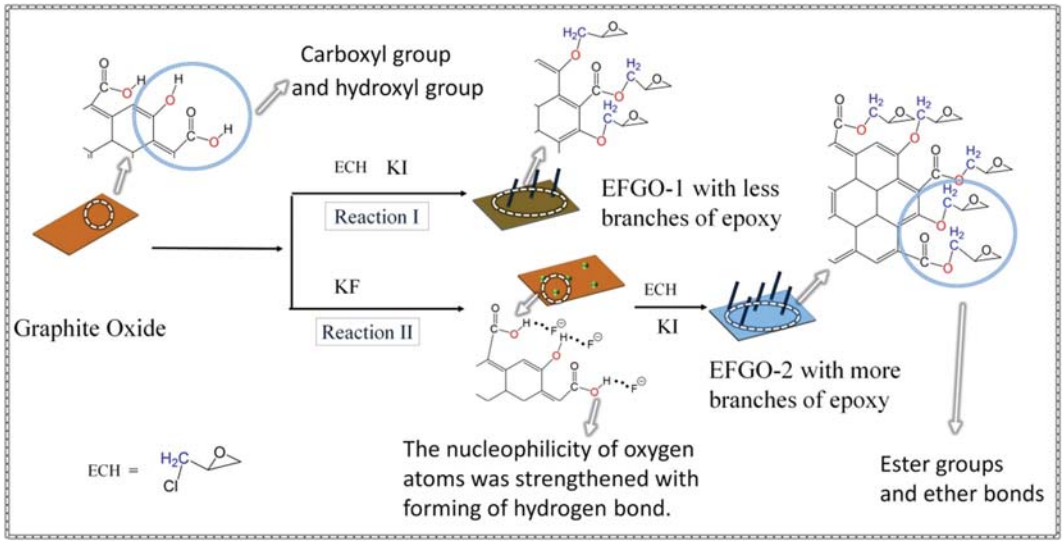

Fig. 1. The principal schematic diagram of grafting reaction of GO with ECH and the change of grafting amount on the surface of GO. (i) It was the formation of hydrogen bonds between the F^- and the active hydrogen of GO surface that made grafting reaction easier between GO and ECH, further improving the grafting amount of epoxypropyl on GO. (ii) The nucleophilicity of oxygen atoms was strengthened with forming of hydrogen bond, so the grafting amount of epoxypropyl on the surface of EFGO-2 was more than that of EFGO-1. (iii) Ester group and ether group had higher decomposition temperature than carboxyl group and hydroxyl group, resulting in the improvement of thermal stability of EFGO.

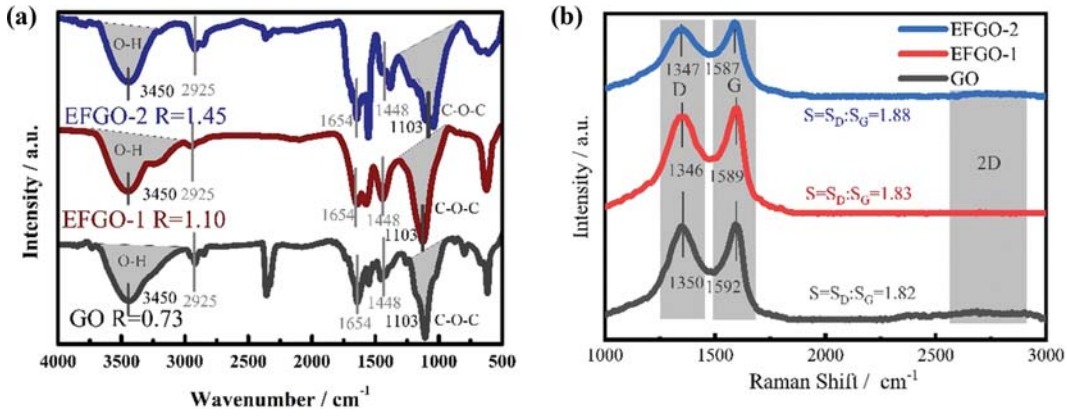

Fig. 2. FTIR spectrum (a) and Raman spectrum (b) of GO before and after grafting ECH.

was open circuit potential (OCP)±0.25 V.

RESULTS AND DISCUSSION

1. Structure of EFGO and Influence of Catalyst on Grafting amount of Epoxypropyl

To improve the compatibility of GO with EP, EFGO was prepared by grafting reaction of GO with ECH under different catalytic conditions. The reaction diagram is shown in Fig. 1.

The FTIR and Raman spectra of EFGO and GO are shown in Fig. 2(a) and (b), respectively. As canbe seen from Fig. 2(a), there were stretch vibration absorption peaks of ether bond (C-O-C) and associated hydroxyl group (O-H···O-H) for GO, EFGO-1 and EFGO-2 at 1,103 cm^{-1} and 3,450 cm^{-1}, respectively. This indicated that there were active epoxy groups and hydroxyl groups (carboxyl or alcohol hydroxyl) on the surface GO before and after grafting. If the ratio of the absorption peak area of the epoxy group and the associated hydroxyl group in the same spectrum was defined as R, it could be found that the R values of EFGO (EFGO-1is 1.10, EFGO-2 is1.45) were significantly higher than that of GO (0.73), which was 1.5 times and 2 times, respectively. Since the surface of EFGO had been washed with ethanol for many times, ECH not involved in grafting reaction had been removed. The larger values of R for EFGO-1 and EFGO-2 indicated that ECH had been successfully grafted to the surface of GO. As further confirmed by the Raman spectrum in Fig. 2(b). According to the literature [17], the D-band at 1,350 cm^{-1} was attributed to sp^3 hybridized state carbon such as the edge-defect (C-OH, C-O-C functionalized epoxy propyl group). The G-band at 1,587 cm^{-1} was ascribed to the in-plane stretching of the ordered sp^2 hybridized states carbon. Similar to the analysis process of infrared spectrum, if the ratio of the peak area of D-band and G-band for the same spectrum was defined as S, it could be found that the values of S for EFGO-2 and EFGO-1 were greater than that of GO. The larger S values also showed that ECH containing much sp^3 hybridized states carbon had been successfully grafted to the surface of GO. In addition, the fact could also be confirmed by the XPS testing results. According to the literature [17,18], the peak of C1s in Fig. 3(a), (c) could be divided into three peaks, which are attributed to C-C peak (~284.8 eV), C-O-C (epoxy/alkoxy) peak (~286.5 eV) and C=O peak (~287.9 eV), respectively. And the peak of O1s in Fig. 3(b), (d) could be divided into two peaks, attributed to C-O-C peak (~532.5 eV) and C=O peak (~530.8 eV), respectively. The content of C and O with different hybridized states for GO and EFGO-2 is shown in the illustration. The data indicated that the content of sp^3 hybridized carbon along with oxygen (belonging to C-O-C ether bond) on the surface of EFGO-2 was significantly higher than that on the surface of GO. It also showed that ECH had been grafted sucessfully on the surface of GO.

The values of both R and S of EFGO-2 were higher than that of EFGO-1, as indicated that the KI-KF catalytic system was more favorable for the grafting reaction of GO with ECH. Therefore, there

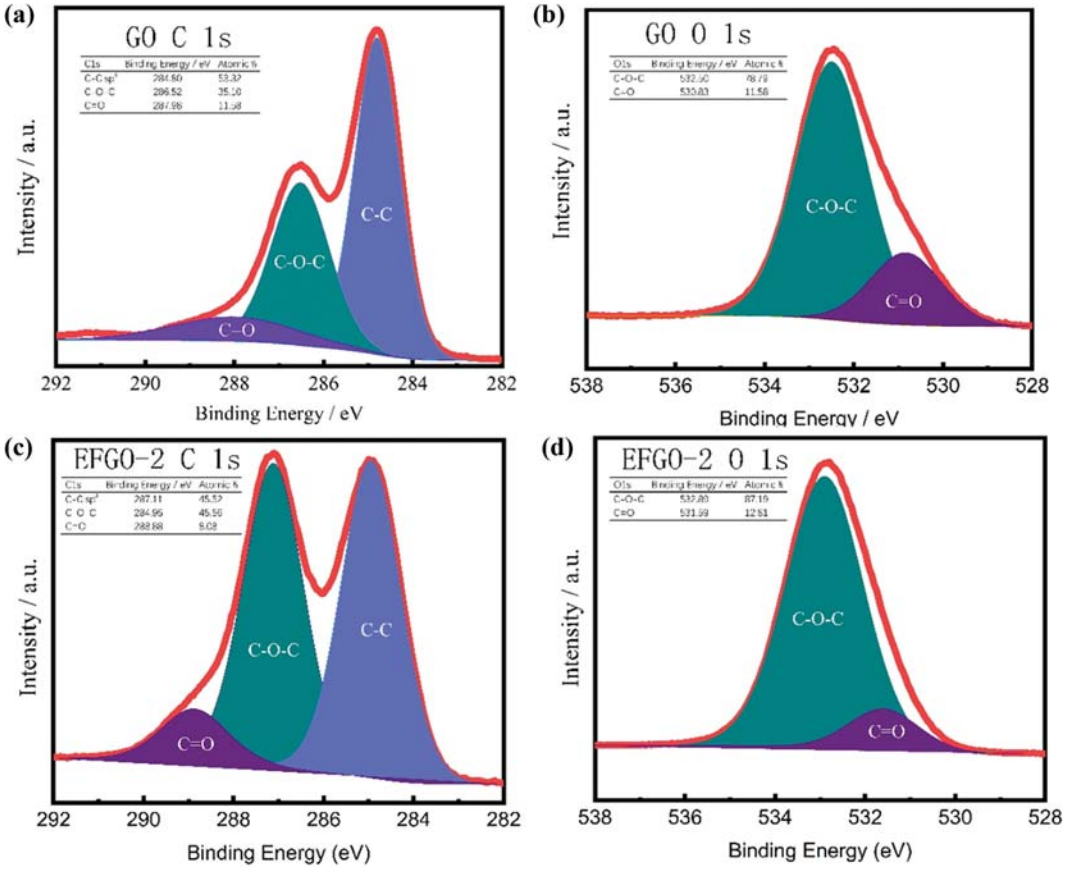

Fig. 3. XPS testing results of GO before and after grafting ECH. (a) C1s of GO, (b) O1s of GO, (c) C1s of EFGO-2, (d) O1s of EFGO-2.

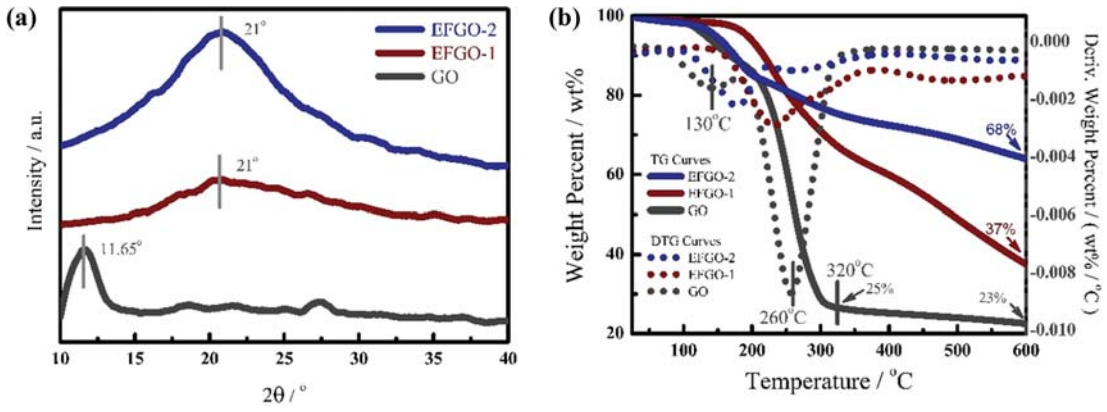

Fig. 4. XRD pattern (a) and TG/DTG curves (b) of GO before and after grafting ECH.

was larger density of epoxy groups on the surface of EFGO-2 than that of EFGO-1.The larger density of epoxy groups would lead to increase of potential reactivity of EFGO, to facilitate covalent bonding between EFGO with DETA (curing agent), to promote the cross-linking among EFGO, DETA and EP. All of them would improve the compatibility between EFGO and EP.

The XRD patterns of two EFGO are shown in Fig. 4(a). Both EFGO-1 and EFGO-2 had diffraction peaks at the same 2θ angle (21°), and the diffraction peak intensity of EFGO-2 was significantly stronger than that of EFGO-1. It might be also related to that more epoxypropyl was grafted uniformly on the surface of GO. TG/DTG curves of GO before and after grafting, shown in Fig. 4(b). It could be seen from DTG curve of GO in Fig. 4(b) that there were two maximum peaks of thermal weight losing for GO at 130 °C and 260 °C, which corresponded to removal of adsorbed water and removal of surface functional group, respectively. When the temperature reached 320 °C, the sample of GO was almost no longer weightless and the residual carbon rate was only 25%. While for EFGO, there was only one maximum peak of thermal weight losing, no weightlessness platform within the test temperature range. At the same pyrolysis temperature, the heat weightlessness rate of EFGO was significantly lower than that of GO, and the heat weightlessness rate of EFGO-2 was lower than that of EFGO-1. Above phenomena indicated that the grafting of epoxypropyl on the GO surface improved the thermal stability of GO. There are two reasons for the increase of EFGO thermal stability after epoxypropyl grafting. First, the grafting reaction reduced the density of the exposed functional groups such as carboxyl and hydroxyl groups on the surface of GO (see Fig. 1). It avoided the decomposition and removal of these groups. The other was that the newly introduced group such as ester group and epoxy group had higher decomposition temperature [19,20]. The fact that the carbon residue rate of EFGO-2 was greater than that of EFGO-1 under the same temperature also proved that KI-KF catalytic system was more favorable for epoxypropyl grafting on the GO surface from another perspective. The content of epoxy group on the surface of EFGO was determined by hydrochloric acid-acetone method [21,22]. The test results showed that the content of epoxy group on the surface of EFGO-2 was up to 7.9×10^{-3} mol/g, higher than that of EFGO-1 (4.4×10^{-3} mol/g) and GO (2.0×10^{-3} mol/g).

Above experimental results show that KF-KI catalysis system was more favorable for grafting of epoxypropyl on GO surface than KI catalysis system. This was because fluoride ion made the nucleophilicity of hydroxyl oxygen or carboxyl oxygen in KF-KI catalysis system enhanced by forming hydrogen bonds with carboxyl and hydroxyl group (See Fig. 1 reaction II) [23]. That is, fluoride ions were conducive to the nucleophilic substitution reaction of hydroxyl oxygen or carboxyl oxygen with carbon atoms of ECH, increasing

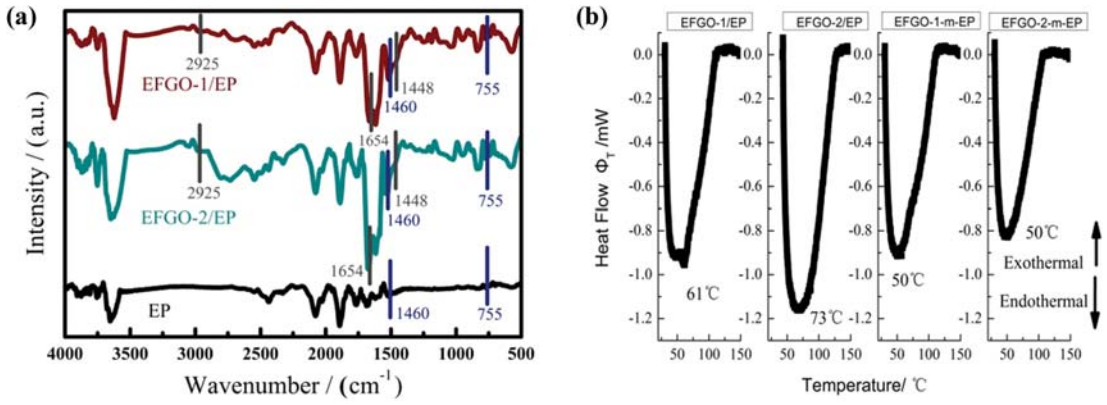

Fig. 5. (a) FTIR spectra of EP, EFGO-1/EP and EFGO-2/EP; (b) DSC curves of EFGO/EP and EFGO-m-EP.

the grafting amount of epoxypropyl on the surface of GO. In addition, the literature [24] also showed that a high concentration of K^+ was also beneficial to increase the nucleophilic substitution rate of hydroxyl oxygen, carboxyl oxygen with halogenated hydrocarbon.

2. Structure of EFGO/EP and Influence of Grafting amount of Epoxypropyl on Compatibility of EFGO with EP

The structure and morphology of EFGO/EP composites were characterized by FT-IR and SEM. The compatibility between EFGO and EP was evaluated by DSC. By comparing the FT-IR spectrum of EFGO-1/EP, EFGO-2/EP and pure EP in Fig. 5(a), it could be found that there were stretching vibration absorption peaks of carbonyl (C=O) at 1,654 cm^{-1} and the bending vibration absorption peaks of hydroxide (O-H) at 1,448 cm^{-1} for both EFGO/EP composites, while there were no above absorption peaks for pure EP. Meanwhile, three characteristic absorption peaks of EP, such as the symmetrical stretching vibration peaks of methyl (-CH_3) at 1,460 cm^{-1}, external bending vibration peaks of C-H bond at 755 cm^{-1}, the stretching vibration absorption peaks of C-H bond at 3,600 cm^{-1} appeared in the FT-IR spectrum of both EFGO/EP composites. This phenomenon indicated that both EFGO were successfully combined with EP.

Cross section SEM images of EFGO-1 and EFGO-2 at low magnification are shown in Fig. 6(a) and (c), respectively. Both EFGO/EP composites sections show large corrugated folds, which is consistent with typical ductile fracture characteristics. A closer observation of the images of EFGO-1/EP at Fig. 6(b) and EFGO-2/EP at Fig. 6(d) in high magnification shows that the sections and fold edges of EFO-2/EP were flat and smooth, while that of EFGO-1/EP was rough and irregular accompanied with stacked particles. At the same time, the inset in Fig. 6(b) also reveals that stacked EFGO flake particles could be found at the fold edge of EFGO-1/EP. These experimental facts demonstrate that EFGO-2 has better apparent compatibility with EP than EFGO-1. We hold the opinion that the compatibility EFGO with EP is related to the content of epoxypropyl on the surface of EFGO. The epoxypropyl of EFGO could react with the curing agent DETA according to the reaction equation in Fig. 7, and further cross-linked with EP to form a network structure with EFGO as the "central node". The content of epoxypropyl in EFGO-2 was higher than that of EFGO-1. Therefore, EFGO-2 could firmly connect with EP chain through multiple covalent bonds resulting in better compatibility between EFGO-2 and EP. On the contrary, there were few or no epoxypropyl on the surface of EFGO-1 particles. This reduced the density of cross linking between EFGO-1 and EP. So EFGO-1 had poor compatibility with EP, and partial EFGO particles dissociated or stacked on the surface of EP.

To further confirm above inference, EFGO and EP were blended by mechanical mixing method. DSC test was conducted on the mixture and EFGO/EP. Fig. 5(b) shows the DSC curves of EFGO-2-m-EP mixture and EFGO-2/EP composite. The glass transition temperature (T_g) and the heat absorption peak [25], which corresponded to glass transition process of typical EP materials, could be found in both EFGO-2/EP and EFGO-2-m-EP. Both glass transition enthalpy (ΔH_g) and heat capacity (c_g) could be calculated by integrating process over the endothermic peak combined with quality of sample according to formulas (1) and (2). The results are shown in Table 1. Here, Φ_T stands for the heat flow rate at temperature T; T_1 and T_2 for initial and termination glass transition temperature, respectively; m for the mass of sample; c_g for heat capacity of sample in the glass transition process.

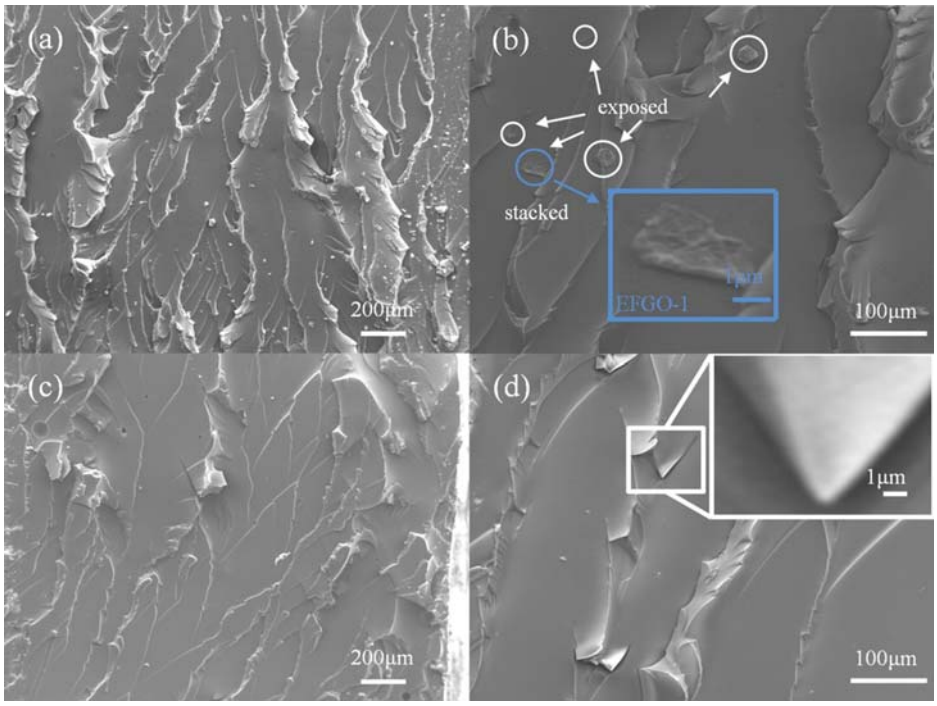

Fig. 6. (a)-(b) SEM image of section morphology for EFGO-1/EP at different magnifications factor; (c)-(d) SEM image of section morphology for EFGO-2/EP at different magnifications factor.

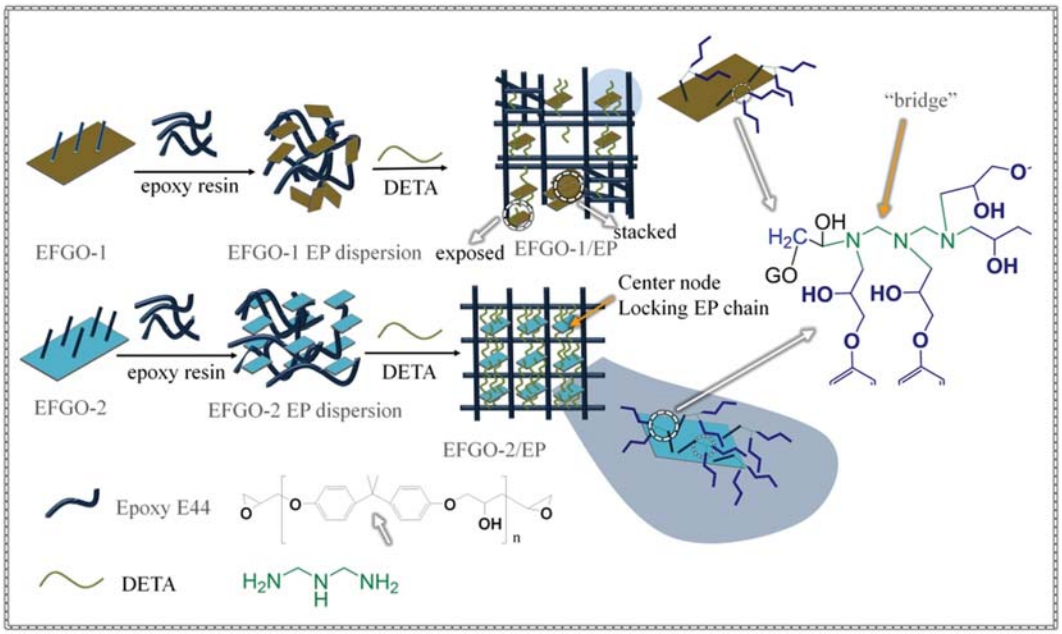

Fig. 7. Schematic diagram of cross-linking reactions between EFGO and EP with DETA as curing agent. During the cross-linking reactions process, EFGO and EP were covalently bonded with DETA, which liked a "bridge". By this sort of "bridge" effect of DETA, the EP segment was locked by EFGO particles effectively and the movement was limited. EFGO-2 with larger grafting amount of epoxypropyl exhibited stronger locked effect than EFGO-1 with smaller grafting amount of epoxypropyl.

Table 1. Thermal parameters in the glass transition process of EFGO/EP composite and EFGO-m-EP mixtures between EFGO and EP

Sample	T_g/°C	m/g	ΔH_g/(J g^{-1})	ΔT/°C	C_g/(J K^{-1} g^{-1})
EFGO-1/EP	61	5.2×10^{-4}	415	30-112	5.07
EFGO-1-m-EP	50	5.1×10^{-4}	409	31-113	5.0
EFGO-2/EP	73	5×10^{-4}	543	36-122	6.31
EFGO-2-m-EP	50	5.2×10^{-4}	342	30-107	4.44

$$\Delta H_g = \int_{T_1}^{T_2} \frac{60\,\Phi_T(T - T_1)}{15\times 1{,}000\times m} \quad (1)$$

$$c_g = \frac{\Delta H_g}{T_2 - T_1} \quad (2)$$

According to the results in Table 1, the T_g of EFGO-2-m-EP blend was 50 °C, which was equivalent to T_g of pure EP. While both T_g (73 °C) and Δh_g (534 J g^{-1}) of EFGO-2/EP composite were higher obviously than that of EFGO-2-m-EP. According to Pattanaik et al. [25], the chain segment of EP moved irregularly in the array when the temperature of material reached T_g, and the order degree of system reduced. The higher T_g of EFGO-2/EP indicated that there were firm covalent bonds between EP chain segment and EFGO-2. The chain segment of EP was "locked" by EFGO-2 (see Fig. 7), making it difficult for EP chain segment to move irregularly. However, the chain segment of EP was "unlocked" in EFGO-2-m-EP. Therefore, the T_g of EFGO-2-m-EP was lower. At the same time, the higher T_g of EFGO/EP also indicated that EFGO was involved in the curing process of DETA and EP and cross-linked with EP to form "central node". It was the crosslinking between EFGO and EP that made the improvement compatibility between EFGO and EP. In addition, the larger heat capacity (c_g) value of EFGO-2/EP than EFGO-2-m-EP also indicated that EFGO-2 was involved and altered the irregular thermal movement of EP chain segment during heating.

Similarly, EFGO-1 was also involved in the curing process of DETA and EP during EFGO-1/EP fabrication. From the perspective of thermal parameters, however, the T_g of EFGO-1/EP was 61 °C, lower than that of EFGO-2/EP. As indicated, the "locking" effect of EFGO-1 on EP segment was weaker than that of EFGO-2.

3. Anticorrosion Evaluations of EFGO/EP

To research the anticorrosive property of EFGO/EP composites, the EFGO/EP coating was prepared on the mild steel by dipping method. The anticorrosion property of coatings was evaluated by EIS and LSV. The Nyquist and Bode diagrams of EFGO-1/EP and EFGO-2/EP are shown in Fig. 8(a) and (b), respectively. The data were fitted using Zview software with circuit $R_{sol}(Q_{coat}(R_{coat}(Q_{dl}R_{CT})))$, and the results are shown in Table 2. Here, R_{sol} stands for solution resistance. R_{coat}, for coating resistance, reflecting the difficulty of electrolyte migration in coating. R_{CT}, for charge transfer resistance, reflecting the difficulty of electron transfer on the surface of mild steel. Because the transport of carriers of electrolyte in both coating and interface of coating/metal was approximately semi-infinite diffusion accompanied with "dispersion effect", two constant phase

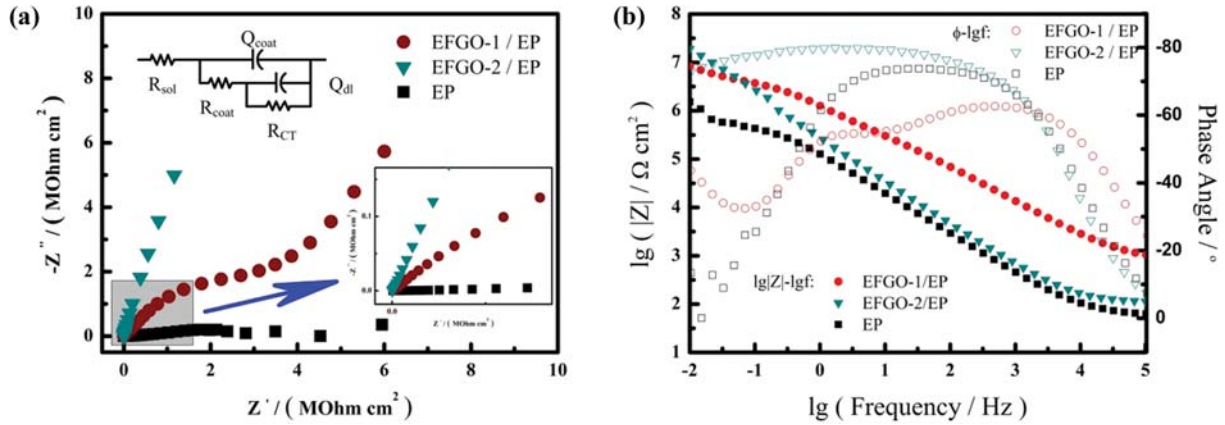

Fig. 8. Nyquist plots (a) and Bode plots (b) of EFGO-1/EP, EFGO-2/EP and pure EP coating in simulated seawater.

Table 2. The fitting results of EIS for EFGO-1/EP and EFGO-2/EP coating at different immersion times

Sample	Immersing time/d	$\|Z\|_{0.01\ Hz}$/ Ω cm^2	R_{sol}/ Ω cm^2	R_{coat}/ Ω cm^2	Q_{coat}		C_{coat}/F cm^{-2}
					Y_0/Ω^{-1} cm^{-2} s^n	n	
EFGO-1/EP	0	8.30×10^6	0.76×10^2	6.01×10^6	1.94×10^{-7}	0.68	14.5×10^{-7}
	14	1.69×10^6	0.99×10^2	9.40×10^5	1.10×10^{-6}	0.82	1.91×10^{-7}
	28	7.05×10^6	1.63×10^2	1.36×10^6	2.19×10^{-6}	0.69	1.33×10^{-7}
EFGO-2/EP	0	1.90×10^7	1.33×10^2	4.88×10^8	6.66×10^{-7}	0.88	2.52×10^{-7}
	14	4.91×10^6	1.17×10^2	1.93×10^6	1.24×10^{-6}	0.83	3.16×10^{-7}
	28	1.22×10^6	1.02×10^2	7.31×10^5	1.04×10^{-6}	0.82	2.45×10^{-7}

Table 3. The coating resistance (R_{coat}), impedance modulus ($|Z|_{0.01\ Hz}$) at 0.01 Hz of EFGO/EP and relevant literature data

Coating	$D_{3.5}$/day	R_{coat}/Ω cm^2	$\|Z\|_{0.01\ Hz}$/Ω cm^2	Ref.
Pure EP	0	3.6×10^5	1.48×10^6	[27]
	14	7.2×10^3	6.03×10^4	
Graphene/EP	0	2.93×10^5	5.62×10^5	[28]
Silane-f-GO/EP	0	9×10^6	1.48×10^7	[29]
GO/EP	0	1.59×10^5	1.99×10^7	[30]
GO/PANi/epoxy	0	7.3×10^6	2×10^7	[31]
Silane-f-GO/silane/epoxy	0	2.35×10^3	2.14×10^4	[32]
Urtica dioica-f-GO/epoxy	0	1.00×10^4	1.25×10^4	[33]

$D_{3.5\%}$ denote the Immersion time of sample in 3.5% NaCl.

angle elements (CPE) denoted as Q_{coat} and Q_{dl}, respectively, were employed to fit the above transport processes. According to the literature [26], the equivalent capacitance of coating (C_{coat}) under the characteristic frequency (ω) could be obtained by substituting the values of Y_0 and n of CPE into formula (3). Here Y_0 and n represent admittance and dispersion strength respectively, The value of C_{coat} could be used to evaluate the content of electrolyte in the coating.

$$C_{coat} = \frac{Y_0}{\omega^{-n+1}\sin\left(\frac{n\pi}{2}\right)} \quad (3)$$

The fitting results showed that the R_{coat} of EFGO-2/EP reached $4.88\times10^8\ \Omega\ cm^2$. The value was two-orders of magnitude larger than that of EFGO-1/EP coating and three-orders of magnitude larger than that of pure EP coating [27], and larger than that of most other similar materials in Table 3 [28-33]. According to the literature [1], the impedance modulus value of coating at 0.01 Hz ($|Z|_{0.01\ Hz}$) could also be used to directly reflect the barrier effect of coating on electrolyte migration. From Table 2, it can be seen that the $|Z|_{0.01\ Hz}$ values of EFGO-1/EP and EFGO-2/EP coating were $8.3\times10^6\ \Omega\ cm^2$ and $1.9\times10^7\ \Omega\ cm^2$, resectively, larger than that of pure EP ($1.53\times10^6\ \Omega\ cm^2$) and were superior to the values of other similar materials (between 10^5 and $10^7\ \Omega\ cm^2$) [28-33] in Table 3.

By comparing the LSV test results of mild steel immersed in simulated seawater in Table 4, it can be found that the values of corrosion voltage (E_{corr}) of mild steel coating with EFGO-1/EP and EFGO-2/EP were 0.21 V and –0.08 V (vs RHE), respectively, which

Table 4. Corrosion voltage and corrosion current density of mild steel coating with EFGO-1/EP and EFGO-2/EP under different immersion times and relevant literature data

Sample	Immersion time/days	i_{corr}/(A cm^{-2})	E_{corr} vs. RHE*/V	Ref.
EFGO-1/EP	0	1.20×10^{-8}	0.21	This work
	14	4.90×10^{-8}	−0.16	
	28	3.72×10^{-7}	−0.16	
EFGO-2/EP	0	5.62×10^{-8}	−0.08	
	14	6.31×10^{-8}	−0.13	
	28	2.09×10^{-7}	−0.11	
Pure EP	0	1.46×10^{-5}	−0.79	[27]
Graphene/EP	0	5.00×10^{-8}	−0.56	[28]
GO/EP	0	1.35×10^{-4}	−0.60	[30]
PANi/GO/epoxy	0	9.0×10^{-6}	−0.39	[31]
PANi-GO/epoxy	0	2.25×10^{-6}	−0.16	[34]
EP coatings with fluorinated polyacrylate	0	7.88×10^{-6}	−0.06	[35]
RGO modified ZnAl-LDH/epoxy	0	2.83×10^{-7}	−0.62	[36]

*The corrosion voltage was versus to reversible hydrogen electrode (E_{corr} vs. RHE).

is higher than that of other similar materials [27,28,30,31,34-36], while the values of corrosion current (i_{corr}) were 1.20×10^{-8} and 5.62×10^{-8} A cm^{-2}, respectively, and comparable to or lower than that of similar materials. Above experimental results showed that both EFFGO/EP coatings had effectively prevented the corrosion ion migrating from electrolyte to the steel plates through coating and improved the anti-corrosion properties of substrate.

By comparing the data in Table 2, the values R_{coat} and $|Z|_{0.01\,Hz}$ of EFGO-2/EP coating were higher than that of EFGO-1/EP coating. And EFGO-2/EP coating exhibited excellent electrolyte barrier. This phenomenon is related to the structure characteristics of EFGO-2, which was synthesized by grafting a large amount of

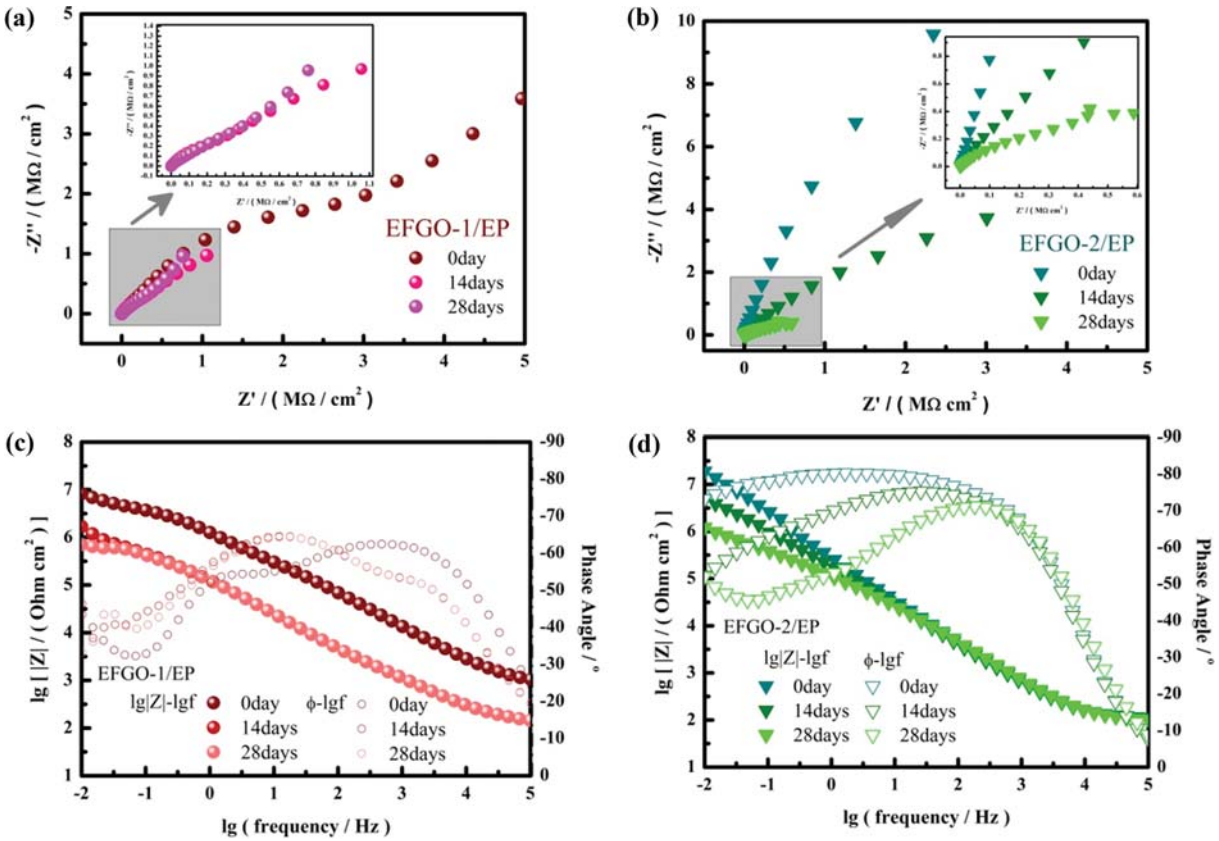

Fig. 9. EIS of mild steel coating with EFGO-1/EP and EFGO-2/EP immersed in 3.5% NaCl for 14 days and 28 days. (a) Nyquist plots of EFGO-1/EP, (b) Nyquist plots of EFGO-2/EP, (c) Bode plots of EFGO-1/EP (d) Bode plots of EFGO-2/EP.

epoxypropyl on the surface of GO. The higher content of epoxypropyl in EFGO-2 improved the compatibility between EFGO-2 and EP. And brought about good hydrophobicity and uniformity of EFGO-2/EP coating. As a result, EFGO-2/EP coating had higher adhesion with mild steel, exhibited strong electrolyte barrier effect. The bode diagrams of the two coatings in Fig. 8(b) also showed that the minimum phase angle of EFGO-2/EP coating was −79.8°, closer to 90° than EFGO-1/EP (−62.6°). The facts further indicated that EFGO-2/EP coating had good hydrophobic properties and strong adhesion to the surface of mild steel [37,38].

4. Influence of Immersion Time on Anticorrosion Property of EFGO/EP

To further investigate the influence of graft amount of epoxypropyl on the anticorrosion durability, the previously used mild steels coating with EFGO-1/EP and EFGO-2/EP were immersed in simulated seawater (3.5 wt% NaCl aq) for 14 and 28 days, respectively. The anticorrosion property was evaluated by EIS and LSV.

Fig. 9(a) and (b) show the Nyquist diagrams of EFGO-1/EP and EFGO-2/EP after immersing for 14 and 28 days, respectively. The data was fitted with circuit $R_{sol}(Q_{coat}(R_{coat}(Q_{dl}R_{CT})))$, and the results are shown in Table 2. It could be seen from the Table 2 that the values of both R_{coat} and $|Z|_{0.01\ Hz}$ of either EFGO-1/EP or EFGO-2/EP coating decreased with the increase of immersion time, except for the value of R_{coat} of EFGO-1/EP after immersing for 28 days was abnormal (this abnormal phenomenon might be caused by large amount of electrolyte infiltrating into the interface between coating and steel plate, and the analog circuit was no longer adapting). The decrease of R_{coat} and $|Z|_{0.01\ Hz}$ indicated that electrolyte had gradually infiltrated into the coating, which reduced the barrier effect of the coating. The values of both R_{coat} and $|Z|_{0.01\ Hz}$ of EFGO-2 were always greater than that of EFGO-1 under same immersing time. These facts showed that the anti-corrosion durability of EFGO-2/EP coating was better than that of EFGO-1/EP coating.

The Bode diagrams of EFGO-2/EP in Fig. 7(d) show there was only one peak at high frequency region for EFGO-2/EP coating, and the minimum phase angle slight deviated by −90° with the extension of immersion time. While, the minimum phase angle of EFGO-1/EP coating in Fig. 7(c) deviated significantly from −90° (−64.5°). These experimental facts demonstrate that two EFGO/EP coatings had partly peeled off from mild steel, and the peeling degree of coating EFGO-1/EP coating was greater than that of EFGO-2/EP coating. During the experiment, the steel plate coated with EFGO-2/EP showed only a small amount of bubbling after immersing in 3.5 wt% NaCl (aq) for 28 days. After removing the coating, the surface of the steel plate was relatively smooth and no obvious corrosion was observed. The steel plate coated with EFGO-1/EP showed more bubbling after immersing for 28 days and linear corrosion marks were observed after removing the coating.

Fig. 10 shows the LSV curves of EFGO-1/EP and EFGO-2/EP after soaking in 3.5 wt% NaCl (aq) for 14 and 28 days, respectively. The corresponding corrosion voltage (E_{corr}) and corrosion current (i_{corr}) data are shown in Table 4, where E_{corr} of EFGO-2/EP was greater than that of EFGO-1/EP and i_{corr} was less than EFGO-1/EP at the same immersing time. The data showed that EFGO-2/EP coating had better long-lasting anticorrosion property than that of

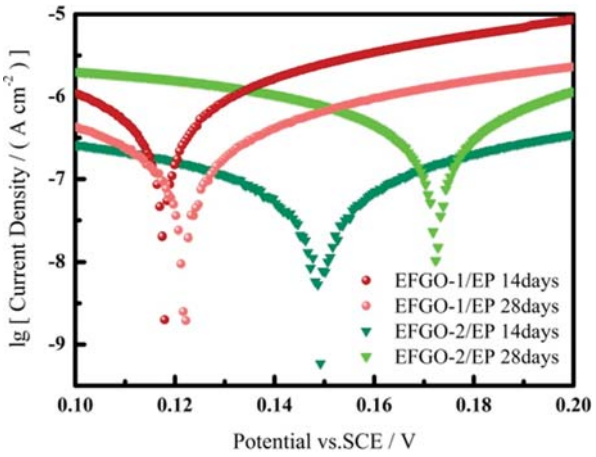

Fig. 10. LSV curves of mild steel coating with EFGO-1/EP and EFGO-2/EP immersed in 3.5% NaCl for 14 and 28 days.

EFGO-1/EP. The long-lasting anticorrosion property of EFGO-2/EP coating was related to its higher graft amount of epoxypropyl in EFGO-2. As mentioned, the higher grafting amount of epoxypropyl on the surface of GO was favorable for cross-linking reaction between EFGO-2 and DETA, which promoted more and firm central nodes of EFGO forming in EFGO-2/EP. It was these more and firm central nodes that had good compability with EP, and given full play to its barrier effect on electrolyte migration in corrosive environment. While the lower grafting amount of epoxypropyl on the surface of EFGO-1 resulted in poor compatibility between EFGO-1 and EP. EFGO-1 partially stacked or exposed in EFGO-1/EP (see Fig. 6(b) SEM image, or Fig. 7 schematic diagram). As brought about that EFGO in EP was prone to migration and slippage in corrosive environment, the long-lasting anticorrosion property of EFGO-1/EP was decreased.

CONCLUSION

Both KI and KI-KF sysems could catalyze the grafting reaction of GO with ECH to obtain EFGO. During the forming of hydrogen bond between GO surface and F^-, however, the grafting amount of epoxypropyl was obiously larger using KI-KF catalytic systems than that using KI systems. As further resulting in improvement of compatibility between EFGO-2 and EP. The EFGO/EP network with EFGO as the "central node", which was formed by cross-linking EFGO with EP, locked the movement of EP chain segment and further improved the thermal stability of EFGO/EP. Meanwhile, the EFGO-2/EP coating fabricated by the EFGO-2, which grafted larger epoxypropyl, had good anticorrosion performance and adhesion with mild steel. EFGO-2/EP coating displayed good blocking effect for migration of corrosion electrolyte, manifesting initial and long-lasting anticorrosion properties under the same corrosion conditions. The coating resistance of EFGO-2/EP reached $4.88\times10^8\ \Omega\ cm^2$.

ACKNOWLEDGEMENTS

This work was supported by Natural Science Foundation of Shanxi

Province China (Grant No. 201801D121066, 201901D111138), Research Project Supported by Shanxi Scholarship Council of China (HGKY2019069), Fund Program for the Scientific Activities of Selected Returned Overseas Professionals in Shanxi Province (2016), The 131 leading talents project of Shanxi province (2016).

REFERENCES

1. G. Cui, Z. X. Bi, R. Y. Zhang, J. G. Liu, X. Yu and Z. L. Li, *Chem. Eng. J.*, ***373***, 104 (2019).
2. F.-L. Jin, X. Li and S.-J. Park, *J. Ind. Eng. Chem.*, **29**, 1 (2015).
3. J. X. Lu, K. S. Moon, B. K. Kim and C. P. Wong, *Polymer*, **48**(6), 1510 (2007).
4. R. Bagheri, B. T. Marouf and R. A. Pearson, *Polym. Rev.*, **49**(3), 201 (2009).
5. K. S. Novoselov, A. K. Geim, S. V. Morozov, D. Jiang, Y. Zhang, S. V. Dubonos, I. V. Grigorieva and A. A. Firsov, *J. Sci.*, **306**(5696), 666 (2004).
6. D.-P. Sui, H.-H. Li, Y. Chai, J. Li, S. Liu, Y. Zhao, H.-T. Fan and H.-B. Xu, *Desalin. Water Treat.*, **94**, 263 (2017).
7. R. Ding, W. H. Li, X. Wang, T. J. Gui, B. J. Li, P. Han, H. W. Tian, A. Liu, X. Wang, X. J. Liu, X. Gao, W. Wang and L. Y. Song, *J. Alloys Compd.*, **764**, 1039 (2018).
8. S. Liu, L. Gu, H. Zhao, J. Chen and H. Yu, *J. Mater. Sci. Technol.*, **32**(5), 425 (2016).
9. Q. Zhu, E. Li, X. Liu, W. Song, Y. Li, X. Wang and C. Liu, *Prog. Org. Coat.*, **140**, 105488 (2020).
10. Q. Zhu, E. Li, X. Liu, W. Song, M. Zhao, L. Zi, X. Wang and C. Liu, *Compos. Part A-Appl. S*, **130**, 105752 (2020).
11. B. Ramezanzadeh, S. Niroumandrad, A. Ahmadi, M. Mahdavian and M. H. M. Moghadam, *Corros. Sci.*, **103**, 283 (2016).
12. C. B. Liu, S. H. Qiu, P. Du, H. C. Zhao and L. P. Wang, *Nanoscale*, **10**(17), 8115 (2018).
13. S. Pourhashem, M. R. Vaezi, A. Rashidi and M. R. Bagherzadeh, *Prog. Org. Coat.*, **111**, 47 (2017).
14. Z. Zhang, W. Zhang, D. Li, Y. Sun, Z. Wang, C. Hou, L. Chen, Y. Cao and Y. Liu, *Int. J. Mol. Sci.*, **16**(1), 2239 (2015).
15. J. Xu, K. Wang, S.-Z. Zu, B.-H. Han and Z. Wei, *Acs Nano*, **4**(9), 5019 (2010).
16. J. H. Lee, S. J. Na, C. D. Yoo and Y. S. Kim, *Sens. Actuators a-Phys.*, **148**(2), 454 (2008).
17. N. You, X.-F. Wang, J.-Y. Li, H.-T. Fan, H. Shen and Q. Zhang, *J. Ind. Eng. Chem.*, **70**, 346 (2019).
18. R. Larciprete, S. Gardonio, L. Petaccia and S. Lizzit, *Carbon*, **47**(11), 2579 (2009).
19. X. Q. Liang, F. Zhang, W. Feng, X. Q. Zou, C. J. Zhao, H. Na, C. Liu, F. X. Sun and G. S. Zhu, *Chem. Sci.*, **4**(3), 983 (2013).
20. G. Zhao, T. Wen, X. Yang, S. Yang, J. Liao, J. Hu, D. Shao and X. Wang, *Dalton Trans.*, **41**(20), 6182 (2012).
21. Z. He, Y. Wang, T. Zhao, Z. Ye and H. Huang, *Anal. Methods*, **6**(12), 4257 (2014).
22. K. Manzoor, M. Ahmad, S. Ahmad and S. Ikram, *Acs Omega*, **4**(17), 17425 (2019).
23. J. H. Clark, *Chem. Rev.*, **80**(5), 429 (1980).
24. X. P. Wang and W. F. Xu, *Bull. Korean Chem. Soc.*, **26**(12), 1923 (2005).
25. A. Pattanaik, M. Mukherjee and S. B. Mishra, *Compos. Part B: Eng.*, **176**, 107301 (2019).
26. C. Fan, J. Shi and K. Dilger, *Prog. Org. Coat.*, **137**, 105333 (2019).
27. S. Pourhashem, M. R. Vaezi, A. Rashidi and M. R. Bagherzadeh, *Corros. Sci.*, **115**, 78 (2017).
28. S. Liu, G. Lin, H. Zhao, J. Chen and H. J. J. o. M. S. Yu, *J. Mater. Sci. Technol.*, **32**(5), 425 (2016).
29. J. Yu, W. Zhao, G. Liu, Y. Wu and D. Wang, *Surf. Topogr.-Metrol.*, **6**(3), 034019 (2018).
30. F. Jiang, W. Zhao, Y. Wu, J. Dong, K. Zhou, G. Lu and J. Pu, *Prog. Org. Coat.*, ***127***, 70 (2019).
31. V. A. Mooss, A. A. Bhopale, P. P. Deshpande and A. A. Athawale, *Chem. Pap.*, **71**(8), 1515 (2017).
32. N. Parhizkar, B. Ramezanzadeh and T. Shahrabi, *Appl. Surf. Sci.*, **439**, 45 (2018).
33. B. Nikpour, B. Ramezanzadeh, G. Bahlakeh and M. Mahdavian, *Corros. Sci.*, **127**, 240 (2017).
34. X. Zhu, Z. Ni, L. Dong, Z. Yang, L. Cheng, X. Zhou, Y. Xing, J. Wen and M. Chen, *Prog. Org. Coat.*, **133**, 106 (2019).
35. Y. Xie, W. Liu, L. Liang, C. Liu, S. He, F. Zhang, H. Shi and M. Yang, *Colloids Surf. A: Physicochem. Eng. Aspects*, **579**, 123659 (2019).
36. D. Yu, S. Wen, J. Yang, J. Wang, Y. Chen, J. Luo and Y. Wu, *Surf. Coat. Technol.*, **326**, 207 (2017).
37. J. Huang, B. G. Sumpter and V. Meunier, *Chem.-Eur. J.*, **14**(22), 6614 (2008).
38. V. K. W. Grips, H. C. Barshilia, V. E. Selvi, Kalavati and K. S. Rajam, *Thin Solid Films*, **514**(1), 204 (2006).